Electronic Supplementary Material (ESI) for Journal of Materials Chemistry B.

Electronic Supplementary Information (ESI)

Naphthalimide based fluorescent organic nanoparticle in selective sensing of Fe^{3+} and as diagnostic probe for Fe^{2+}/Fe^{3+} transition

Deblina Sarkar, Monalisa Chowdhury and Prasanta Kumar Das*

School of Biological Sciences, Indian Association for the Cultivation of Science
Jadavpur, Kolkata – 700032, India.

*To whom correspondence should be addressed: bcpkd@iacs.res.in

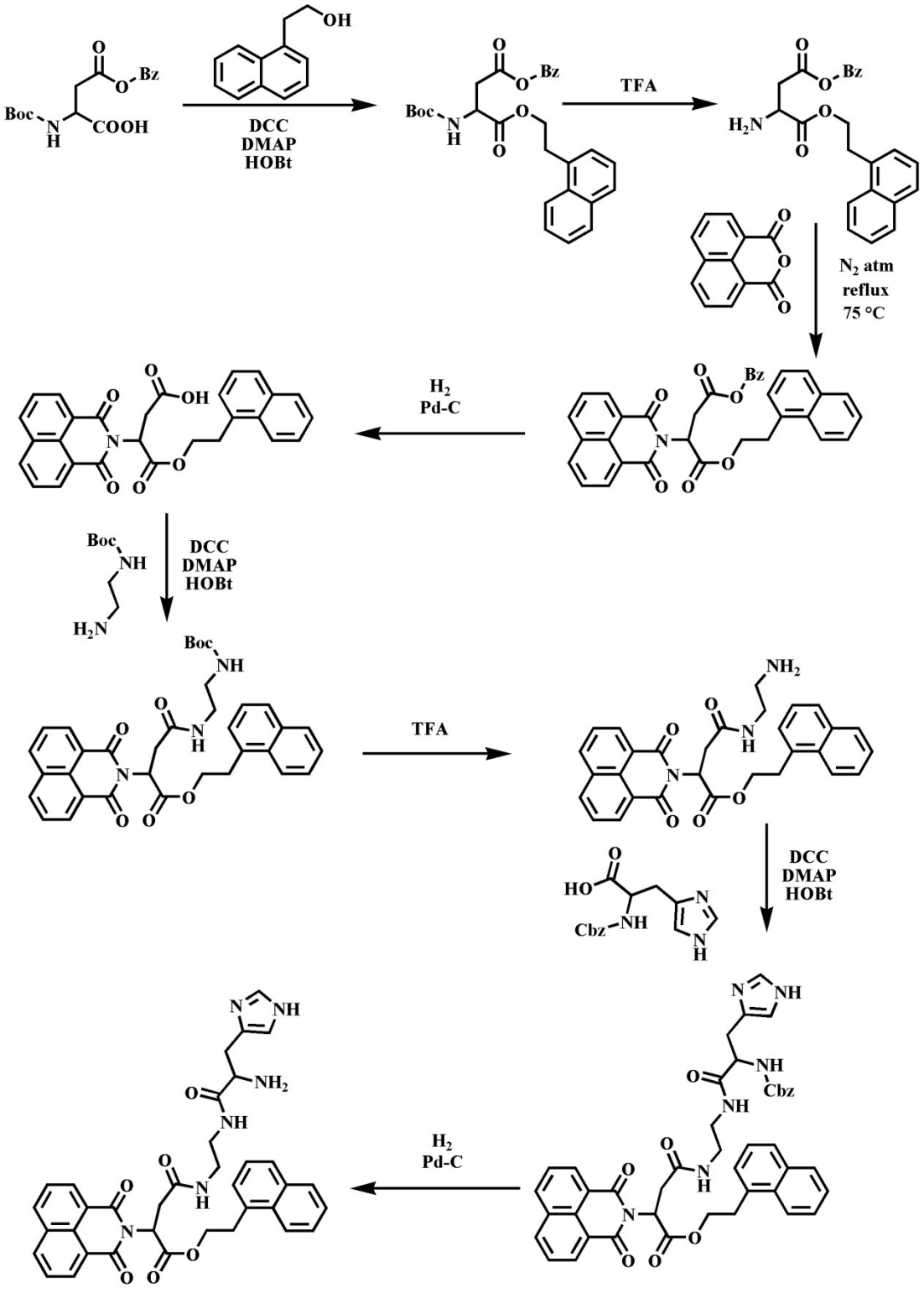

Scheme S1. Synthetic scheme of **NID**.

Table S1 Comparison of Fe^{3+} sensors.

Probes	LOD	Response type	References
Rhodamine-based probe	0.1 μM	Fluorescence turn on	*Chem. Commun*., 2010, **46**, 1407-1409.
Boron-dipyrromethene (BODIPY) based fluorescence probe	1.3×10^{-7} M	Fluorescence turn on	*ACS Appl. Mater. Interfaces,* 2014, **6**, 18408-18412.
Triphenylamine based probe	1.44 μM	AIE based Fluorescence turn off	*J. Mater. Chem. C,* 2016, **4**, 383-390.
Carbon quantum dots/block copolymer ensembles	8.37 μM	Fluorescent sensing	*J. Mater. Chem. B,* 2017, **5**, 5397
carbon nanoparticles	0.55 ppm	Fluorescent sensing	*J. Mater. Chem. A,* 2015, **3**, 136-138
AgNp	2 μM	Localised surface plasmon resonance	*Colloids Surfaces A,* 2018, **555**, 324-331.
Cyclodextrin Supramolecular Complex	1 μM	FRET-based ratiometric sensor	*Langmuir*, 2010, **26**, 4529-4534.
Naphthalene based sensor	3.53×10^{-5} M	Fluorescence turn off	*Tetrahedron Lett*, 2010, **51**,3962-3965.
Rhodamine-based polymeric film sensor	1 μM	FRET-based ratiometric fluorescent sensing	*Sens. Actuators B Chem.,* 2010, **145**, 451-456.
Anionic poly(3,4-propylenedioxythiophene) derivative based sensor	0.023 mM	Colorimetric Sensor	*Sens. Actuators B Chem.*, 2017, **244**, 891-896
Anionic Zn-based MOF	0.0233 mM	Fluorescent sensing	*Dalton Trans.,* 2018, **47**, 3452-3458.
Naphthalimide derivative	**12.5±1.2 μM**	**Fluorescent Turn Off**	**Present Study**

Characterization of **NID.**

^{1}H-NMR (400 MHz, $CDCl_3$, 25 °C): δ/ppm: 8.500-8.539 (m, 3H, C-3, C-8 proton of naphthalimide, C-2 proton of imidazole), 8.365-8.389 (m, 2H, C-5, C-6 proton of naphthalimide), 7.853-7.964 (m, 4H, C-4, C-5, C-8 protons of naphthyl ring, C-5 proton of imidazole), 7.608-7.639 (m, 2H, C-4, C-7 protons of naphthalimide), 7.418-7.438 (d, 1H, C-7 proton of naphthyl ring), 7.336-7.372 (t, 1H, C-6 proton of naphthyl ring), 7.154-7.285 (m, 1H, C-3 proton of naphthyl ring), 6.967-7.005 (m, 1H, C-2 proton of naphthyl ring), 6.239-6.274 (m, 1H, chiral centre of L-aspartic acid residue), 5.071-5.091 (m, 2H, O-C$\underline{H}_2$-CH_2-$C_{10}H_7$), 4.453-4.497 (m, 1H, chiral centre of L-histidine residue), 3.489-3.569 (m, 6H, -N-C$\underline{H}_2$-C$\underline{H}_2$-N- and O-CH_2-C$\underline{H}_2$-$C_{10}H_7$), 3.274-3.366 (m, 2H, methylene protons of L-histidine residue), 2.969-3.029(m, 2H, methylene protons of L-asparticacid residue).^{13}C-NMR (400 MHz, $CDCl_3$): 170.48, 168.95, 160.68, 135.43, 134.55, 134.15, 133.55, 132.24, 131.95, 131.79, 128.98, 127.61, 127.44, 127.25, 127.16, 127.12, 126.16, 125.77, 125.63, 123.78, 119.08, 63.19, 50.05, 49.38, 36.35, 29.65, 28.97. MALDI-TOF: m/z: 647.69 [M+H]+(calculated); 647.039 (found). $[\alpha]_D^{25}$ = -13.78° (c = 0.58g/100mL) in $CHCl_3$).

Real time bioimaging.

We carried out real time bioimaging experiment for normal cells (NIH3T3) and cancer cells (B16F10) in 4 well chamber slides. First we incubated both type of cells separately in different chamber slides for 24 h (5% CO_2) at 37 °C. Followed by we incubated **NID** FONPs in (25 μM, f_w = 99 vol%) in both type of cells for 3 h and carried out fluorescence imaging. We took the cells within chamber slides again in the CO_2 incubator for another 3 h and carried out the same experiment till overall 6 h incubation of the FONPs. After that we incubated Fe^{2+}(250 μM) and Fe^{3+}(250 μM) separately in different wells of chamber slides where compound was already incubated. Subsequently, we carried out the imaging experiment for 6 h incubation of Fe^{2+} and Fe^{3+} included within both type of cells.

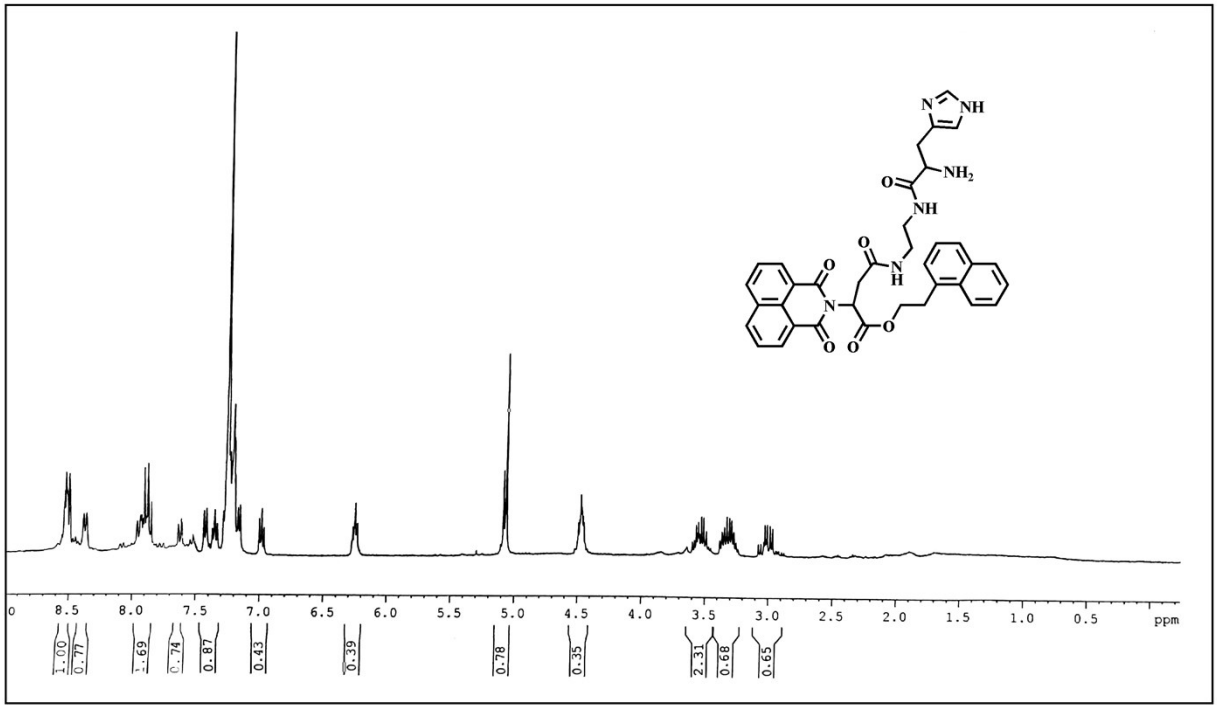

Fig. S1. ^{1}H-NMR spectrum of **NID**.

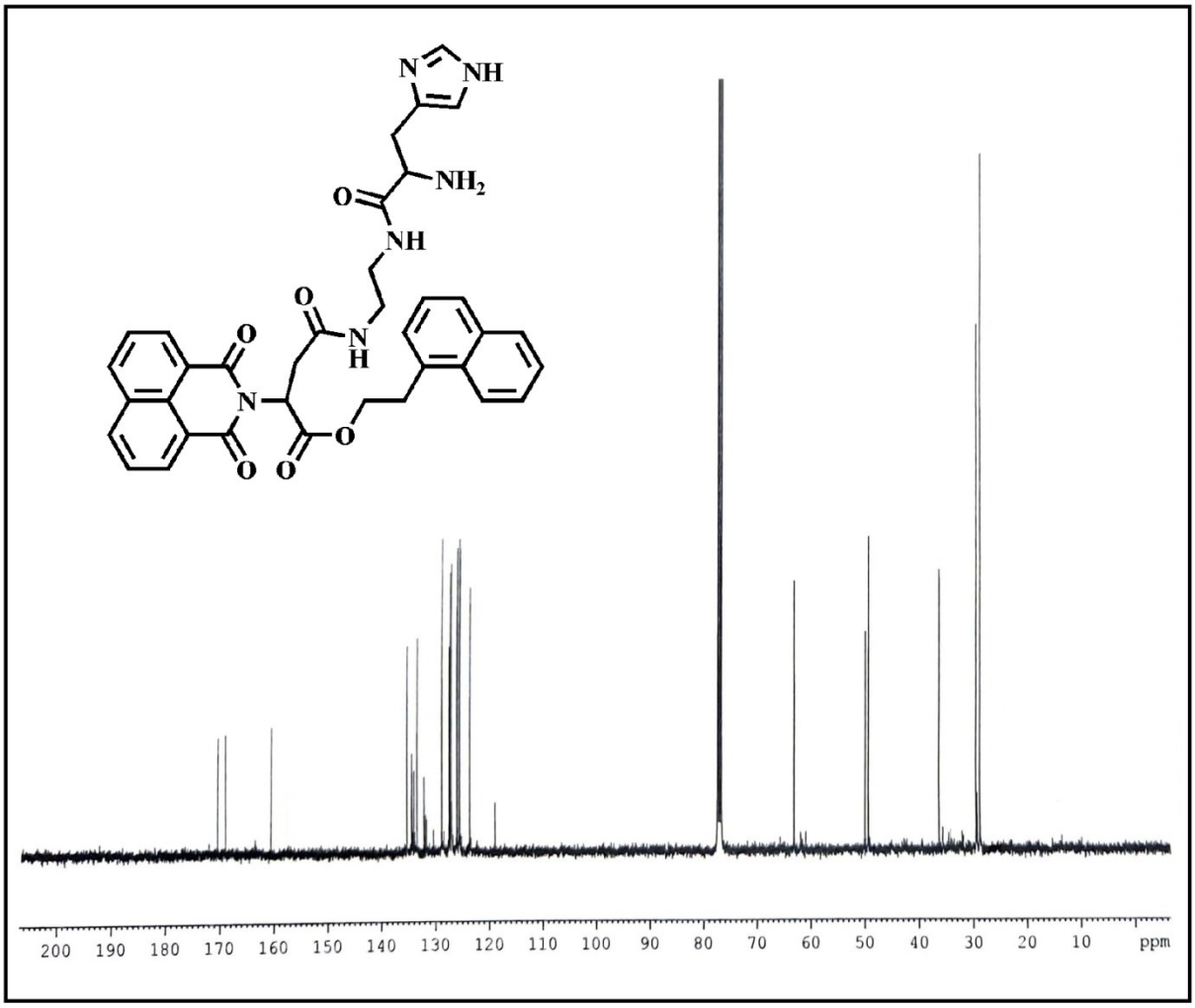

Fig. S2. ^{13}C-NMR spectrum of **NID**.

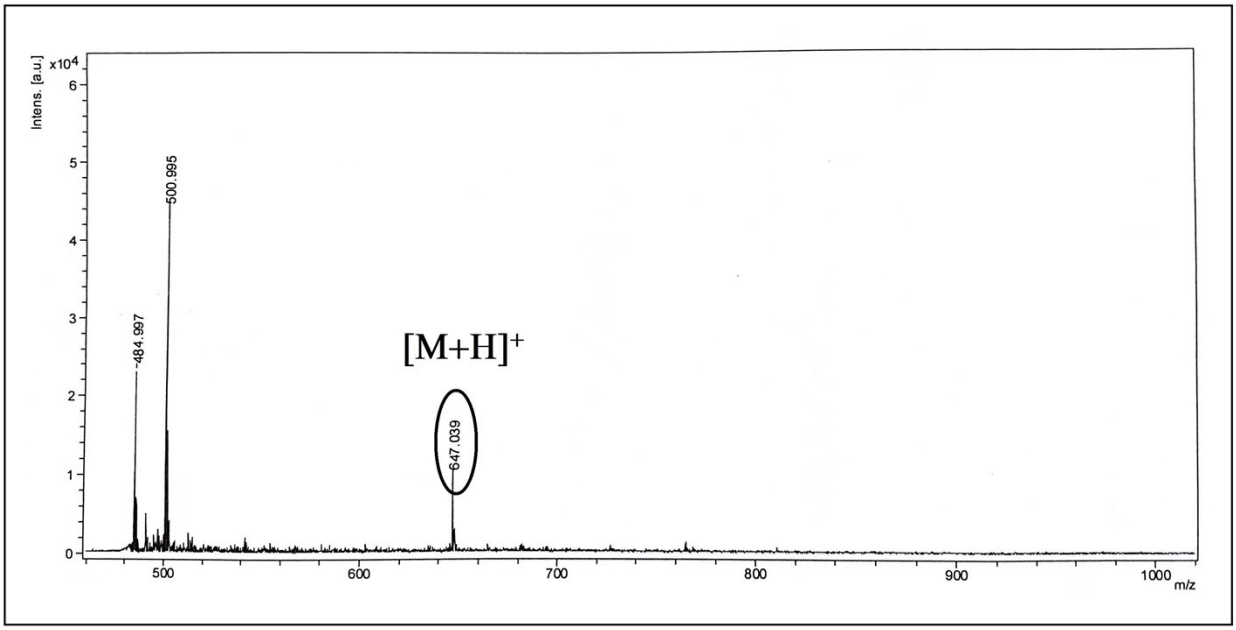

Fig. S3. Mass spectrum of **NID**.

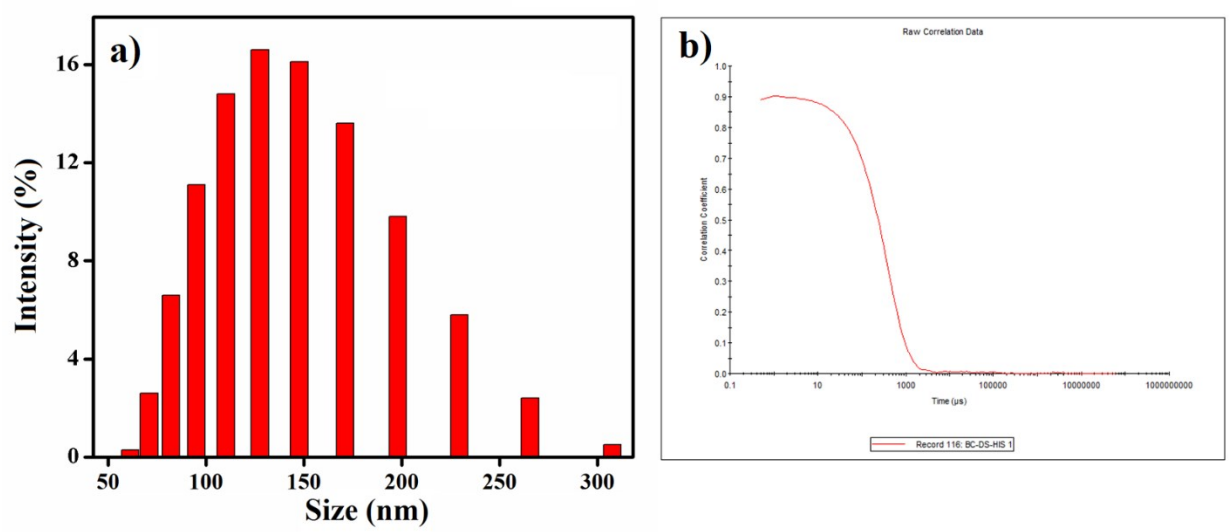

Fig. S4. (a) DLS plot of particles size distribution (intensity averaged), (b) correlogram obtained by DLS of **NID** in (1:99, v/v) DMSO-water binary solvent mixture ([**NID**] = 10 μM).

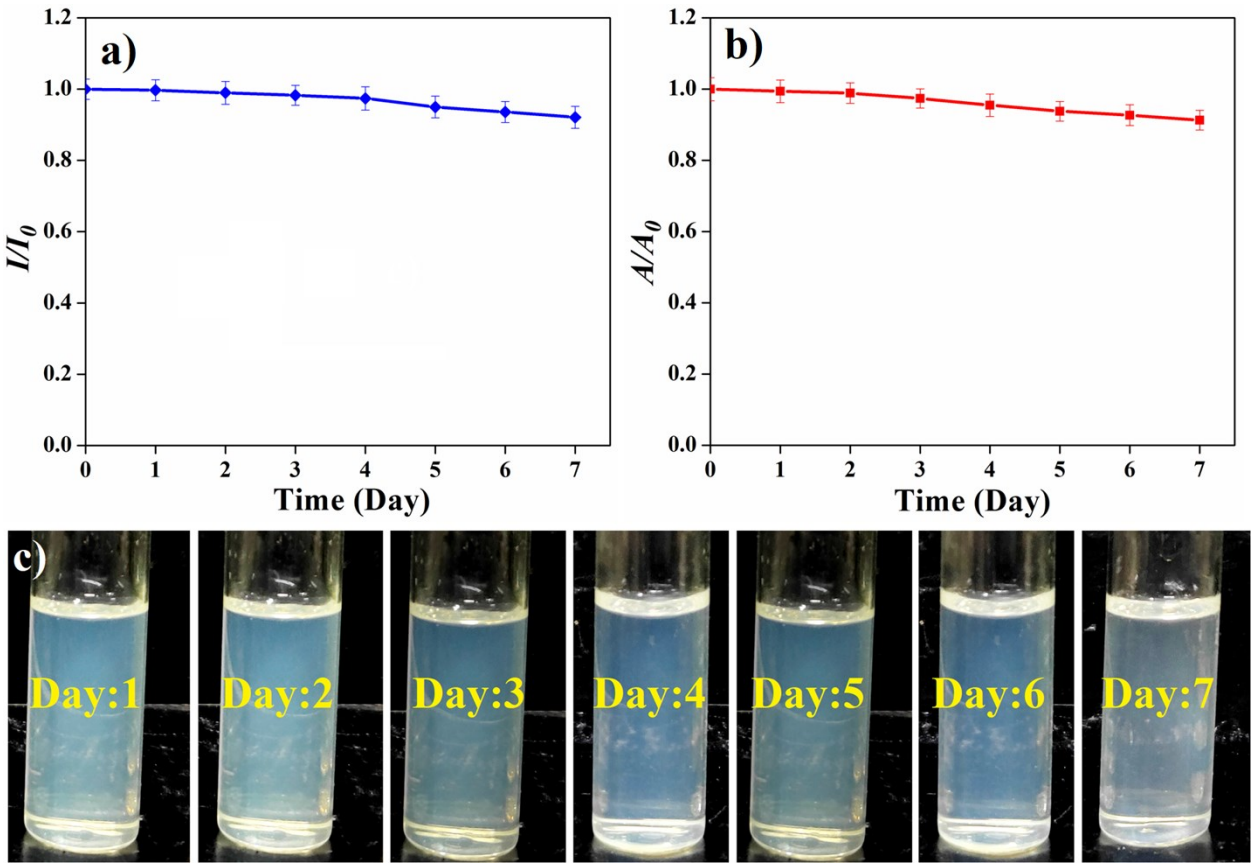

Fig. S5. Ratio of (a) absorbance value, (b) fluorescence intensity over time for **NID** FONP at f_w = 99 vol% in DMSO. (c) photographs of **NID** FONP solution for 7 days.

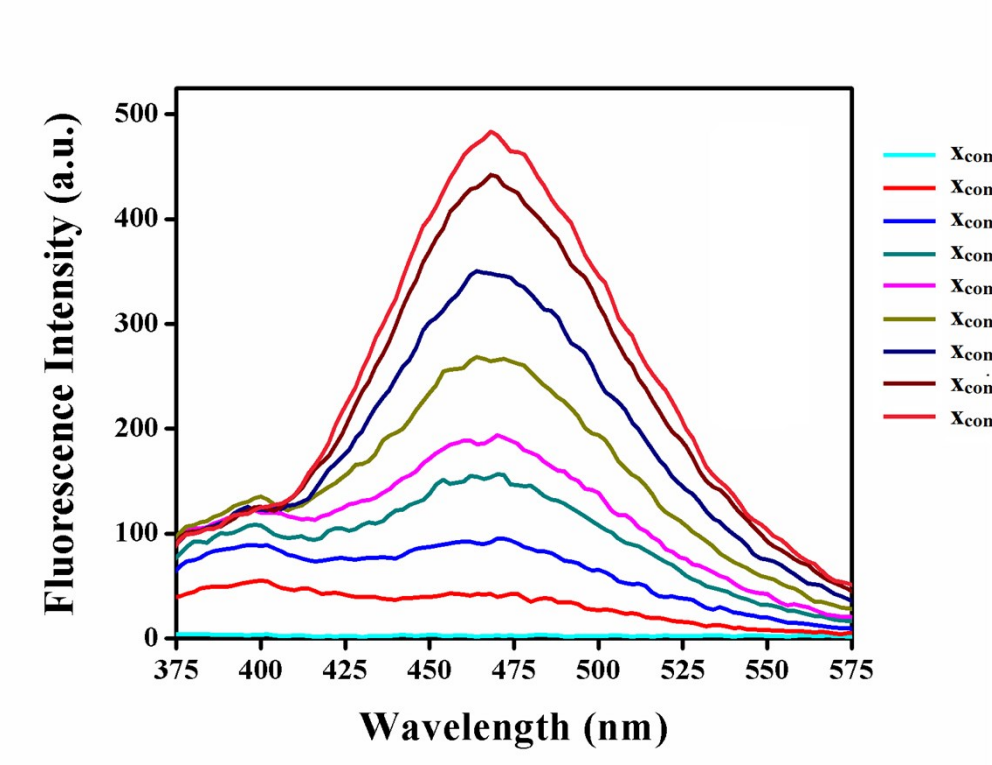

Fig. S6. Emission spectra of different mole fraction of **NID** / Fe^{3+}in 1:99 (v/v) DMSO-water. X_{comp} = Mole fraction of **NID**.

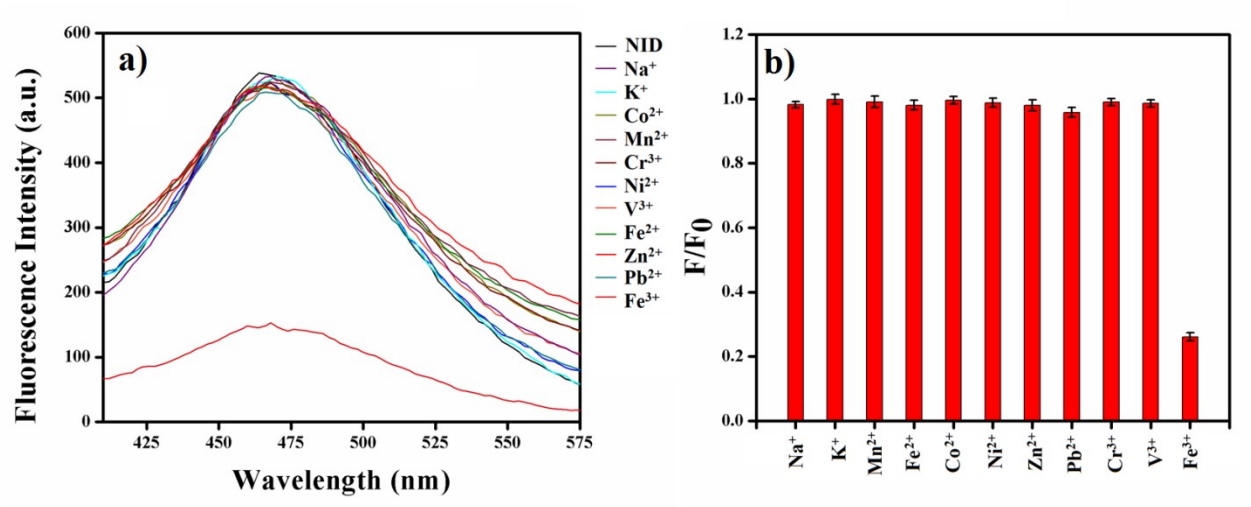

Fig. S7. Selectivity of **NID** FONPs ([**NID**] = 50 μM) to Fe^{3+} over other metal ions [metal] = 500 μM in (1:99, v/v) DMSO-water solution. (a) Fluorescence intensity plot (b) relative intensity of **NID** FONPs in presence of different metal ions. The error bars represent the standard deviations.

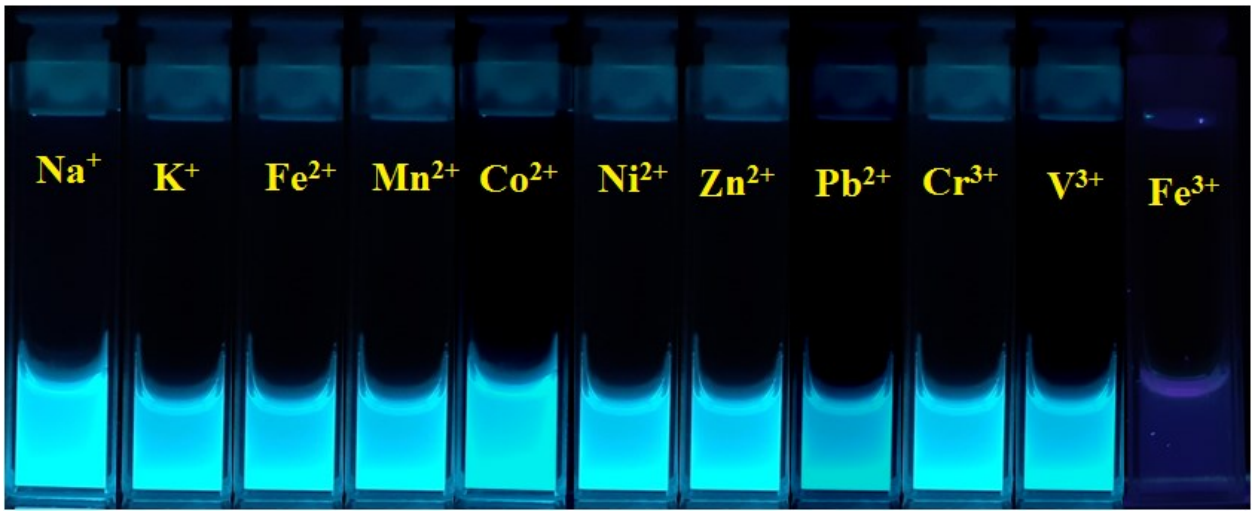

Fig. S8. Photograph of selectivity of **NID** FONPs ([**NID**] = 50 μM) to Fe^{3+} over other metal ions (500 μM) in (1:99, v/v) DMSO-water solution upon UV-light irradiation (λ_{ex} = 365 nm).

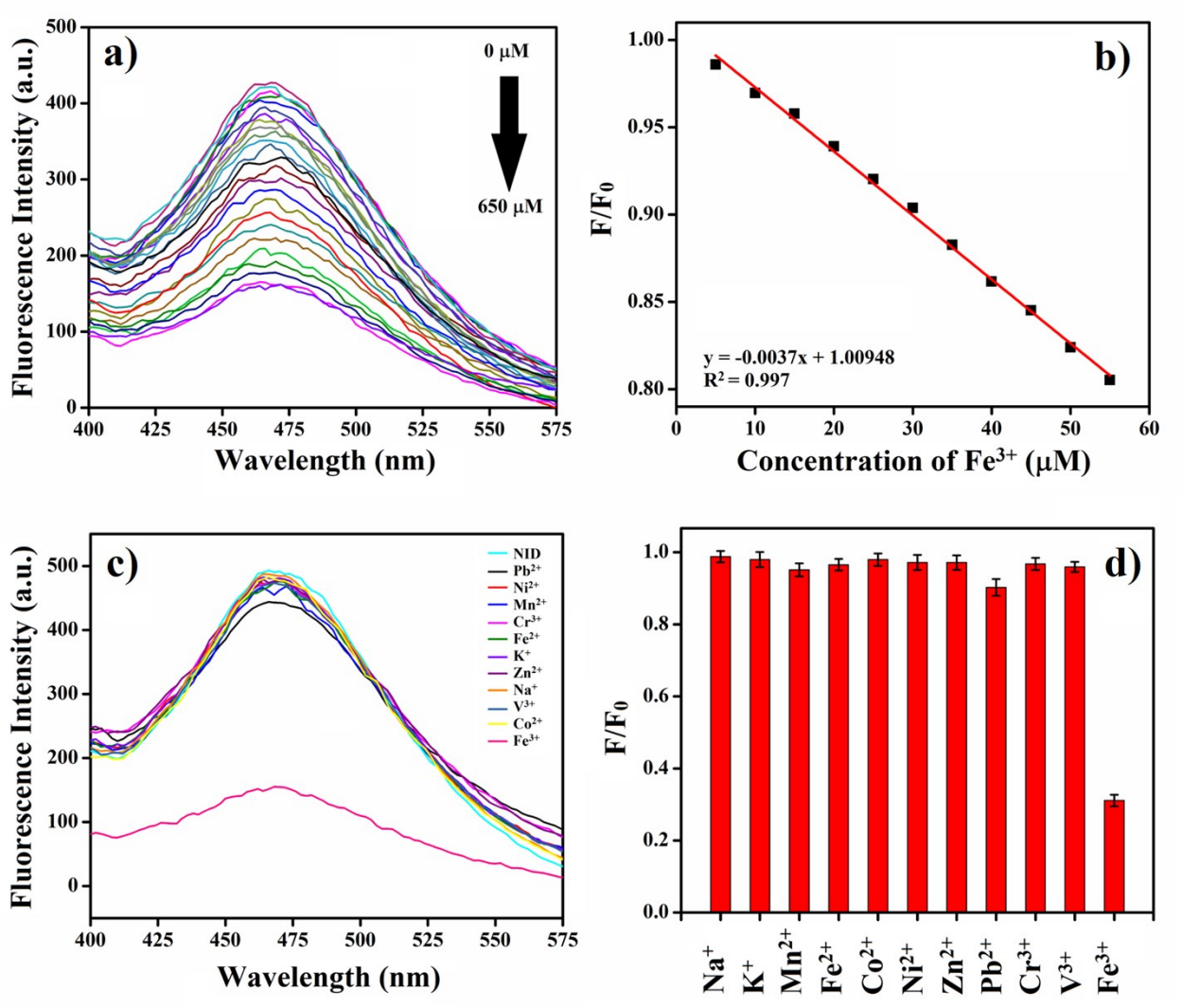

Fig. S9. (a) Fluorescence spectra of **NID** FONPs (50 μM) in absence and presence of varying concentration of Fe^{3+} (excitation wavelength = 350 nm), (b) Stern-Volmer plot of Fe^{3+} doped in (1:99, v/v) DMSO-aqueous phosphate buffer (10 mM, pH = 7.4) solution of **NID** (50 μM), Selectivity of **NID** FONPs ([**NID**] = 50 μM) to Fe^{3+} over other metal ions [metal] = 500 μM in (1:99, v/v) DMSO-aqueous phosphate buffer (10 mM, pH = 7.4) solution. (c) Fluorescence intensity plot (d) relative intensity of **NID** FONPs in presence of different metal ions. The error bars represent the standard deviations.

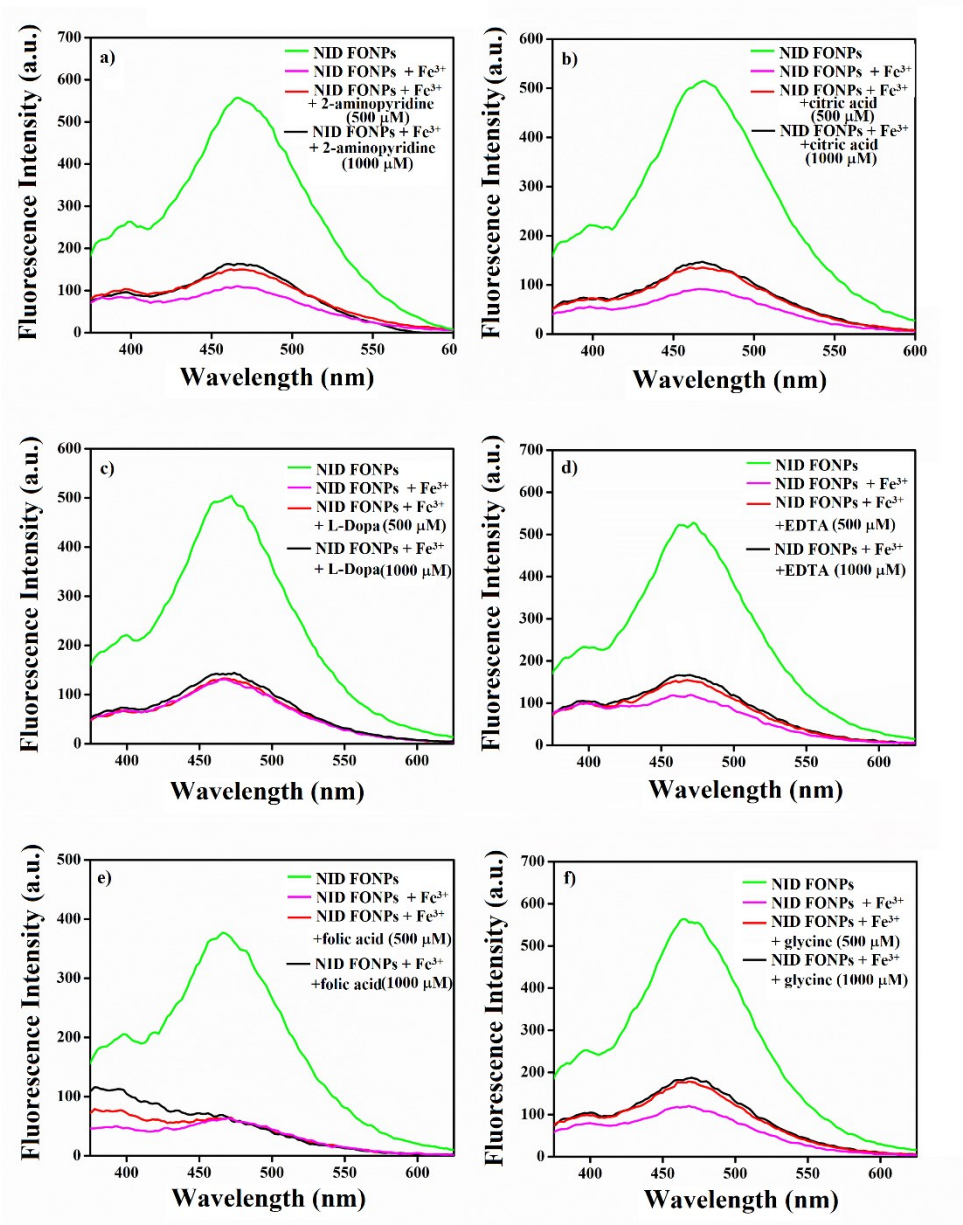

Fig. S10. Emission spectra of of **NID** FONPs (50 µM) and mixture of **NID** FONPs (50 µM) + Fe^{3+} (500 µM) in absence and presence of 500 & 1000 µM of (a) 2-aminopyridine, (b) citric acid, (c) L-Dopa, (d) EDTA, (e) folic acid and (f) glycine.

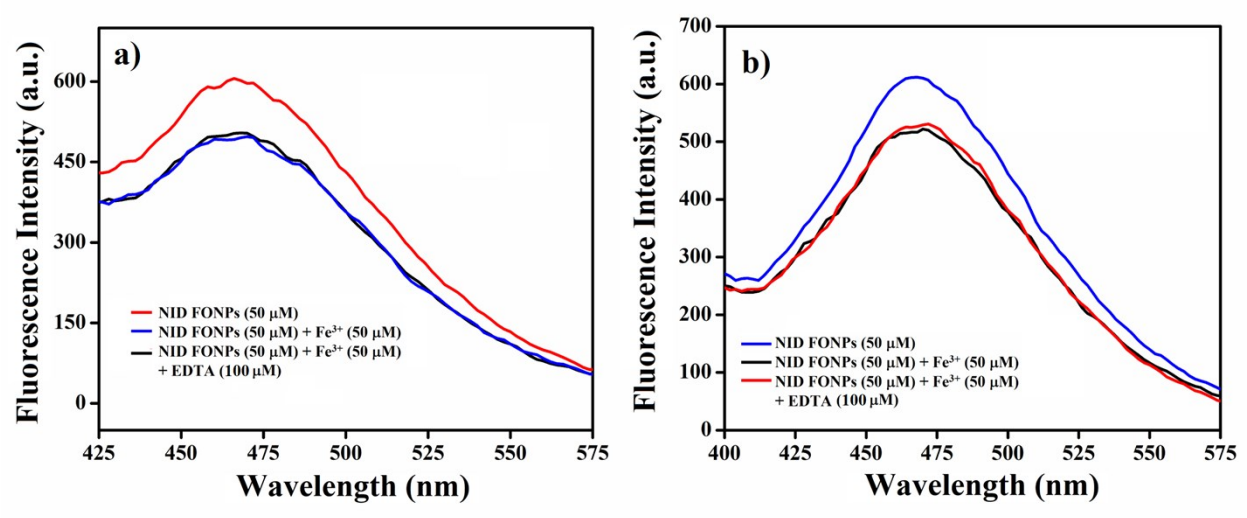

Fig. S11. Emission spectra of **NID** FONPs (50 μM) and mixture of **NID** FONPs (50 μM) + Fe^{3+} (50 μM) in absence and presence of 100 μM EDTA in (a) Milli-Q water and (b) aqueous phosphate buffer (pH = 7.4, 10 mM).

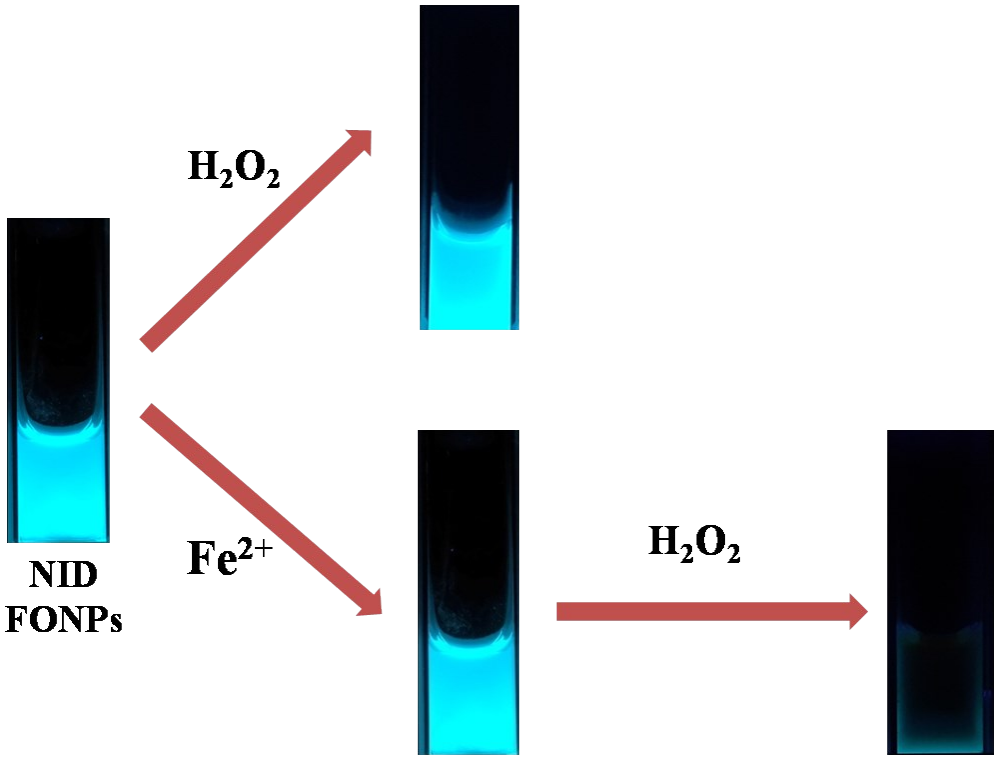

Fig. S12. Photographs **NID** FONPs ([**NID**] = 50 μM), **NID** FONPs + Fe^{2+} ([**NID**] = 50 μM, [Fe^{2+}] = 500 μM), **NID** FONPs + H_2O_2 ([**NID**] = 50 μM and [H_2O_2]= 500 μM) and **NID** FONPs + Fe^{2+} + H_2O_2 ([**NID**] = 50 μM, [Fe^{2+}] = 500 μM and [H_2O_2] = 500 μM) in (1:99, v/v) DMSO-water solution upon UV-light irradiation (λ_{ex} = 365 nm).

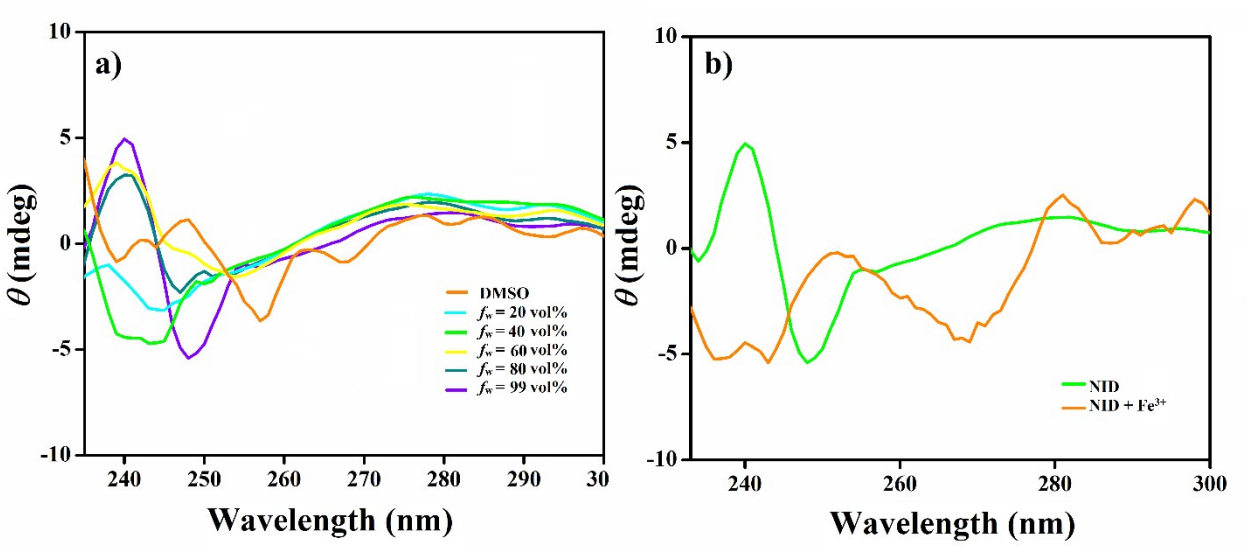

Fig. S13. CD spectra of (a) **NID** (500 μM) in different ratios of DMSO-water, (b) **NID** (500 μM) at f_w = 99% in DMSO in presence of Fe^{3+} (5 mM).

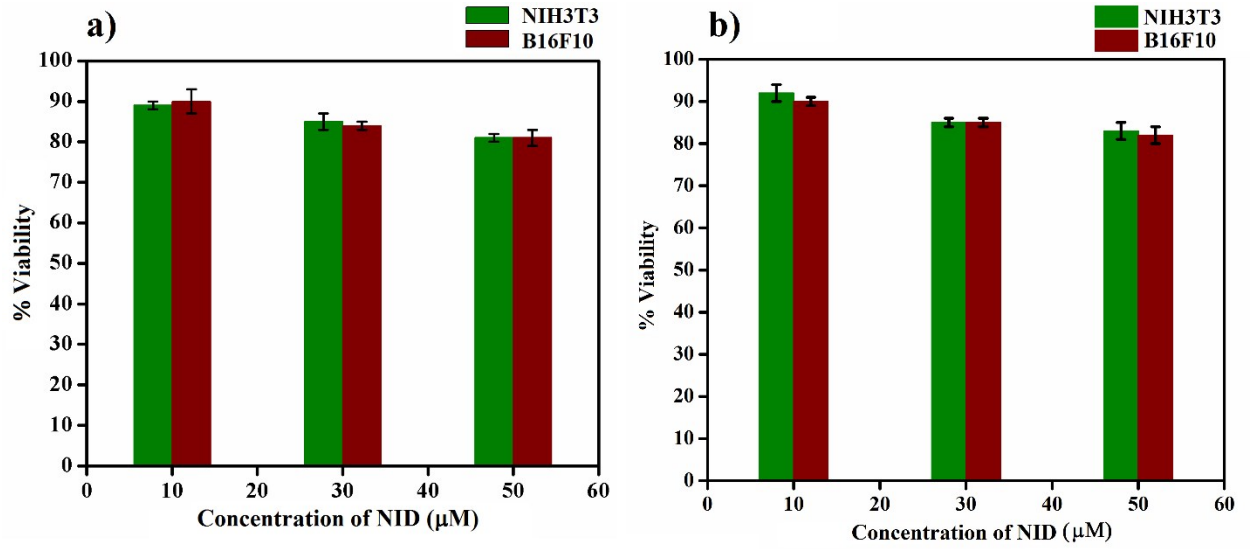

Fig. S14. MTT-based % cell viability of NIH3T3 (non-cancer cells) and B16F10 (cancer cells) in presence of varying concentration of FONPs derived from **NID** in 1:99 v/v, DMSO-water over the incubation period of (a)12 h, (b) 24 h. Percent errors are within ± 5% in triplicate experiments.

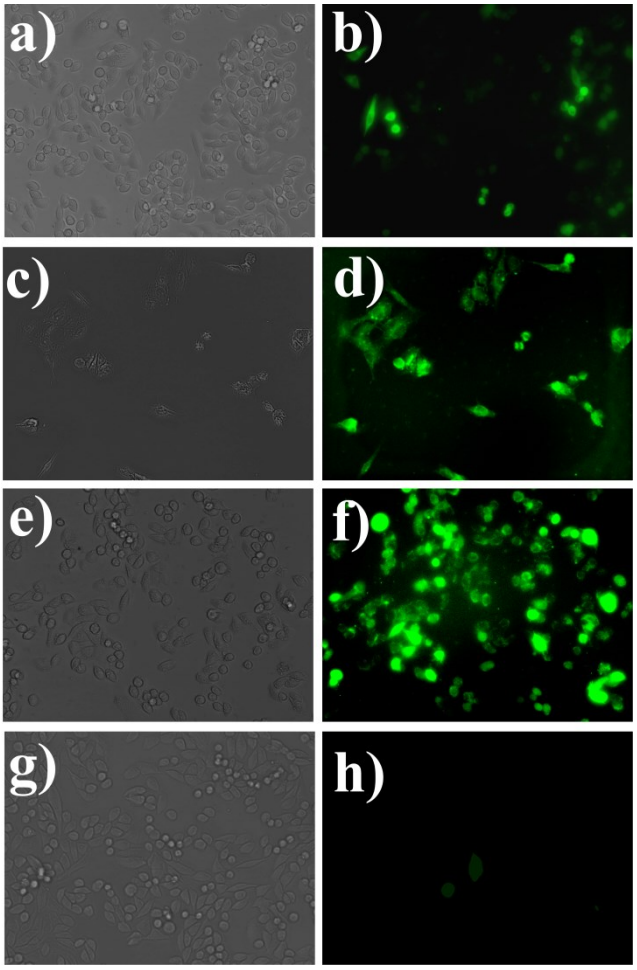

Fig. S15. Bright-field, fluorescence microscopic images of NIH3T3 cells after incubation with **NID** FONPs (25 μM) for 3 h (a,b) and 6 h (c,d) , incubation with **NID** FONPs (25 μM) + Fe^{2+}(250 μM), (e, f) **NID** FONPs (25 μM) + Fe^{3+}(250 μM) (g, h) for 6 h.

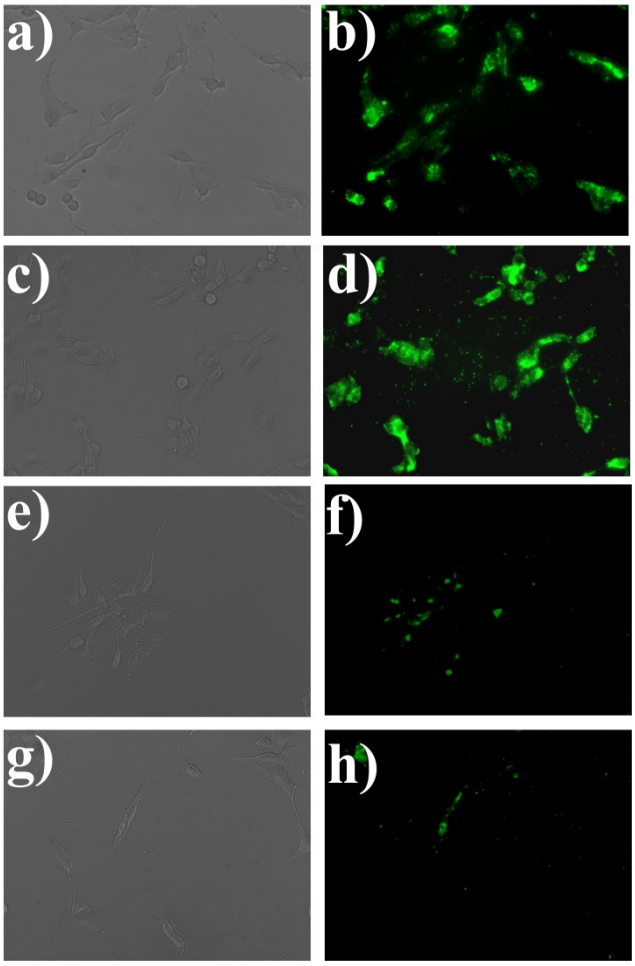

Fig. S16. Bright-field, fluorescence microscopic images of B16F10 cells after incubation with **NID** FONPs (25 μM) for 3 h (a,b) and 6 h (c,d), incubation with **NID** FONPs (25 μM) + Fe^{2+}(250 μM), (e, f) **NID** FONPs (25 μM) + Fe^{3+}(250 μM) (g, h) for 6 h.

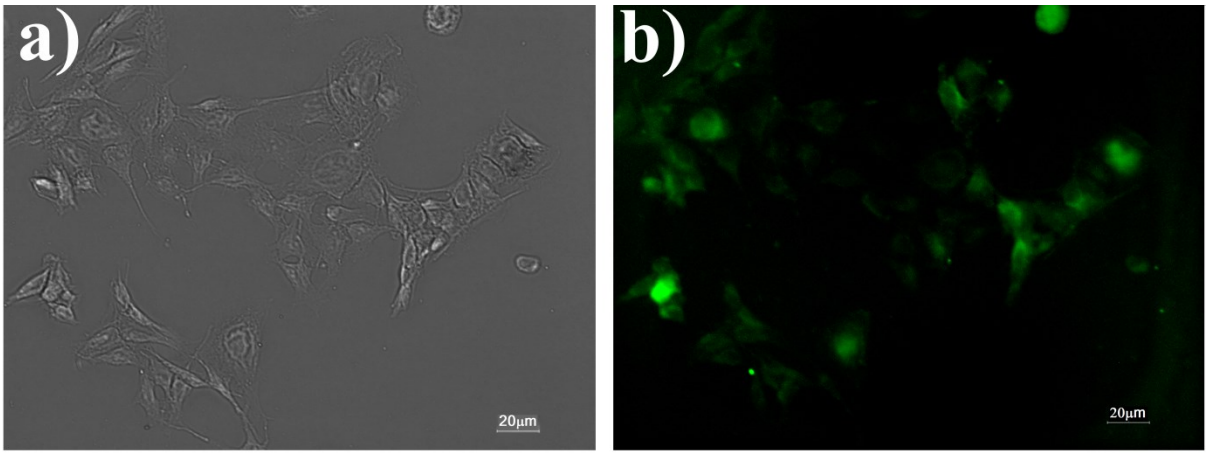

Fig. S17: a) Bright-field, b) fluorescence microscopic image of co-cultured NIH3T3 and B16F10 cells after 6 h incubation with **NID** FONPs (25 μM) + Fe^{2+} (250 μM).